Microwave-induced amplitude- and phase-tunable qubit-resonator coupling in circuit quantum electrodynamics

S. Zeytinoğlu, M. Pechal,* S. Berger, A. A. Abdumalikov Jr., A. Wallraff, and S. Filipp†
Department of Physics, ETH Zurich, 8093 Zurich, Switzerland
(Received 13 February 2015; published 30 April 2015)

In the circuit quantum electrodynamics architecture, both the resonance frequency and the coupling of superconducting qubits to microwave field modes can be controlled via external electric and magnetic fields to explore qubit-photon dynamics in a wide parameter range. Here, we experimentally demonstrate and analyze a scheme for tuning the coupling between a transmon qubit and a microwave resonator using a single coherent drive tone. We treat the transmon as a three-level system, with the qubit subspace defined by the ground and the second excited states. If the drive frequency matches the difference between the resonator and the qubit frequencies, a Jaynes-Cummings-type interaction is induced, which is tunable in both amplitude and phase. We show that coupling strengths of about 10 MHz can be achieved in our setup, limited only by the anharmonicity of the transmon qubit. This scheme has been successfully used to generate microwave photons with a controlled temporal shape [M. Pechal *et al.*, Phys. Rev. X **4**, 041010 (2014)] and can be directly implemented with superconducting quantum devices featuring larger anharmonicity for higher coupling strengths.

DOI: 10.1103/PhysRevA.91.043846 PACS number(s): 42.50.Pq, 42.50.Ct, 03.67.Lx

I. INTRODUCTION

The interaction between an atom and a single electromagnetic field mode leads, in the simplest case, to an exchange of single energy quanta. This process is commonly described by the Jaynes-Cummings (JC) Hamiltonian $ga^\dagger\sigma + \text{H.c.}$, where the ladder operator $a^\dagger$ creates an excitation in the mode, while σ simultaneously de-excites the atom. The strength g of this coupling is determined by the dipole moment of the atom and the mode volume of the field. Although in free space the interaction is typically weak, it can be enhanced by confining the field to a small volume in a cavity quantum electrodynamics (QED) setting. This field has seen tremendous progress [1–3] and has diversified from the traditional setting with real atoms to solid-state realizations using nanoscale electronic devices such as quantum dots [4,5] and superconducting circuits [6–8] as artificial atoms. However, in most solid-state settings the coupling strength between the atom and the cavity modes is fixed by the geometry of the device and the position of the artificial atom in the cavity, neither of which can be modified *in situ*. Although in recent years, superconducting circuit devices which allow *in situ* access to the amplitude of the qubit-resonator coupling g have been realized [9–12], the phase of g is fixed in these systems. A scheme for controlling this phase, which is equivalent to choosing the field quadrature the qubit couples to, has only recently been demonstrated, in our earlier work [13]. Because of this direct phase tunability, our scheme does not rely on additional frequency-tuning elements to achieve full control over the phase of the resonator field, in contrast with other techniques demonstrated in recent experiments [14,15]. The scheme described here is expected to be useful in a variety of settings, such as performing quantum gate operations [16], creating shaped photons for quantum networks [13,17,18], measuring the vacuum state of a cavity [19], exploring vacuum-induced Berry phases [20], enabling the controlled coupling of a single or multiple qubits to multiple resonator modes [21–23], and engineering quantum reservoirs [24].

The amplitude and phase tunability of the qubit-resonator coupling strength can be achieved by a two-photon process, known as a cavity-assisted Raman process, which has been extensively studied for Λ systems [25–29] and ladder-type (Ξ) systems [30]. Cavity-assisted Raman processes employ an external coherent drive with a time-dependent amplitude $\Omega\cos(\omega_d t + \phi)$ to induce an effective coupling $\tilde{g}$ between the qubit and the resonator degrees of freedom. The experimental access to the amplitude (Ω) and the phase (ϕ) of the external drive enables *in situ* amplitude and phase tunability of this effective qubit-resonator coupling.

Cavity-assisted Raman processes can be readily applied to superconducting circuit elements of the transmon type [31], which are in widespread use because of their excellent coherence properties and the relative simplicity of their fabrication. These circuit elements realize an anharmonic oscillator system, i.e., a system in which transitions are allowed only between neighboring states and the transition frequencies differ from each other by multiples of a small negative parameter α which characterizes the anharmonicity. In experiments using the circuit QED architecture, not only the transition between the ground $|g\rangle$ and the first excited $|e\rangle$ state at frequency ω_{ge}, but also transitions between higher lying energy levels can easily be addressed [32] and complex quantum states can be realized [33]. In particular, the second excited state $|f\rangle$, which is separated from $|e\rangle$ by $\omega_{ef} = \omega_{ge} + \alpha$, has been used widely for quantum gates [34–37] and plays an important role in our implementation of the cavity-assisted Raman processes in a circuit QED setting.

In our experiments, we investigate the tunability of a cavity-assisted Raman-process-induced coupling between a microwave resonator and a transmon device whose qubit states are defined as the ground and second excited states.

*mpechal@phys.ethz.ch
†Present address: IBM T. J. Watson Research Center, Yorktown Heights, New York 10598, USA

We demonstrate the amplitude tunability of the transmon-resonator coupling and analyze the effects of the small anharmonicity of the transmon on the rate and fidelity of the population exchange (SWAP) between the transmon and the resonator, thereby complementing our experiments in which shaped microwave photons were created and analyzed [13].

The outline of the paper is as follows. In Sec. II we present spectroscopic measurements of the tunable coupling strength $\tilde{g}$ using a transmon-type superconducting qubit. In Sec. III, we derive an analytical expression for $\tilde{g}$ using first-order perturbation theory in the drive amplitude Ω. In Sec. IV, we explain an iterative method for calculating the drive-induced ac Stark shift of the qubit levels. In Sec. V, we use numerical simulations and second-order perturbation theory to analyze the fidelity of the excitation exchange between the transmon and the resonator induced by the tunable coupling.

II. SPECTROSCOPIC MEASUREMENT OF THE TUNABLE TRANSMON-RESONATOR COUPLING

Our system consists of a transmon-type superconducting qubit with maximal Josephson coupling energy $E_J^{\max}/h = 47.3$ GHz and charging energy $E_C/h = 0.343$ GHz. We operate the transmon at a transition frequency of $\omega_{ge}/2\pi = 8.103$ GHz, which is higher than the fundamental mode frequency, $\omega_r/2\pi = 7.126$, GHz of the resonator, resulting in a positive transmon-resonator detuning $\Delta = \omega_{ge} - \omega_r = 2\pi \times 0.977$ GHz. With a coupling strength $g/2\pi = 65$ MHz between the transmon g-e transition and the fundamental resonator mode, the system is far into the dispersive regime ($\Delta \gg g$). The transmon has an anharmonicity $\alpha/2\pi = -0.376$ GHz, and the frequency of the transition between the first and the second excited state is $\omega_{ef} = \omega_{ge} + \alpha = 2\pi \times 7.727$ GHz. The resonator decay rate $\kappa/2\pi$ is measured to be 6.6 MHz.

A tunable effective JC-like coupling between the transmon state $|f\rangle$ and the resonator can be activated by applying a coherent microwave tone at a frequency close to the energy difference between the dressed states $|f0\rangle_D$ and $|g1\rangle_D$. Here, the subscript D denotes the dressing of the combined eigenstates $|f0\rangle \equiv |f\rangle \otimes |0\rangle$ and $|g1\rangle \equiv |g\rangle \otimes |1\rangle$ by the transmon-resonator coupling g. The effective coupling leads to a coherent excitation exchange between the transmon and the resonator. The fidelity of this exchange is maximum when the transmon drive frequency ω_d is equal to ω_d^0, which is defined by the resonance condition

$$\omega_d^0 = 2\omega_{ge} + \alpha - \omega_r + \Delta_{f0g1}(\Omega). \tag{1}$$

Thus, ω_d^0 is the angular frequency difference between $|f0\rangle_D$ and $|g1\rangle_D$ modified by the difference $\Delta_{f0g1}(\Omega)$ between the ac Stark shifts for $|f0\rangle_D$ and $|g1\rangle_D$, which depends on the amplitude of the coherent drive Ω.

The strength of the effective transmon-resonator coupling $\tilde{g}$ is measured by weakly probing the frequency-dependent transmission through the resonator [6]. In the strong-coupling regime, the transmission peak of the resonator splits into two distinct peaks of equal width when the resonance condition in Eq. (1) is satisfied, as observed in the measurement data shown in Figs. 1(a) and 1(b). The frequency separation between the two maxima in transmission then equals $2\tilde{g}/2\pi$, i.e., twice the coupling strength between the states $|f0\rangle_D$ and $|g1\rangle_D$.

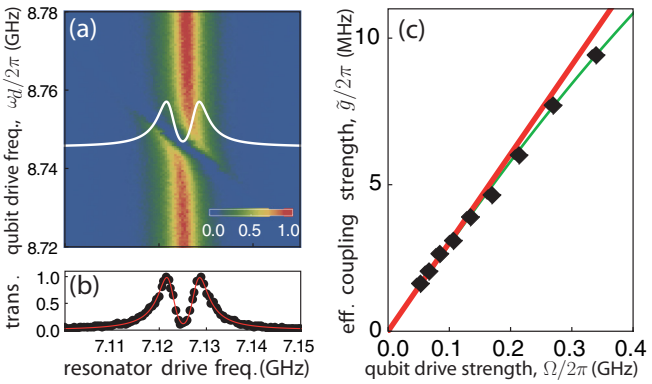

FIG. 1. (Color online) (a) Resonator transmission as a function of the transmon and resonator drive frequencies. The white curve is a fit to the data at the fixed transmon drive frequency $\omega_d/2\pi = 8.75$ GHz. (b) Normalized transmission data for the white fit curve in (a). The amplitude of the effective coupling strength $\tilde{g}/2\pi$ extracted from this trace is 3.1 MHz. (c) Measured effective coupling $\tilde{g}$ (black diamonds) as a function of the coherent drive amplitude Ω: perturbation theory prediction [thick (red) line] and numerical simulations [thin (green) line].

To extract the effective coupling, we first identify the transmon drive frequency ω_d^0 at which the transmission curve is split into two peaks of identical width. We then fit the resonator transmission curve to the response function of the transmon-resonator system given by

$$S(\omega_d) = A_0^2 \left| \frac{i\,|\gamma|\,\omega - \tilde{\omega}^2}{4\tilde{g}^2\left(\omega_d^0\right)^2 - (i\,|\gamma|\,\omega - \tilde{\omega}^2)(i\,|\kappa|\,\omega - \tilde{\omega}^2)} \right|^2 \tag{2}$$

derived from the master equation of the coupled transmon-resonator system in a truncated basis [38]. In Eq. (2), γ is the qubit decay rate, and $\tilde{\omega}^2 = \omega^2 - (\omega_d^0)^2$.

We have measured the coupling strength $\tilde{g}$ for increasing amplitude of the coherent drive strength Ω [see Fig. 1(c)]. When the drive is weak, the effective coupling strength $\tilde{g}$ increases linearly with the amplitude of the drive strength, in good agreement with a first-order perturbation theory calculation outlined in Sec. III. However, for drive amplitudes higher than approximately 0.2 GHz, higher order effects start to contribute significantly and the dependence of $\tilde{g}$ on Ω becomes nonlinear, making the $\tilde{g}$ smaller than predicted by the linear model. The measured strength of the tunable coupling shows good agreement with the numerical simulation [Fig. 1(c); thin solid (green) line] and the analytical result from a perturbation theory calculation to first order in Ω [Fig. 1(c); thick solid (red) line], which are discussed in the following. All system parameters which are relevant to the calculations were extracted from separate experiments. The drive amplitude seen by the transmon qubit was calibrated by fitting the Ω dependence of Δ_{f0g1}. The calibration routine for the coherent drive strength is further discussed in Sec. IV.

III. CALCULATING THE COUPLING STRENGTH $\tilde{g}$

In a reference frame rotating at frequency ω_d, the Hamiltonian for a transmon coupled to a resonator mode can be written

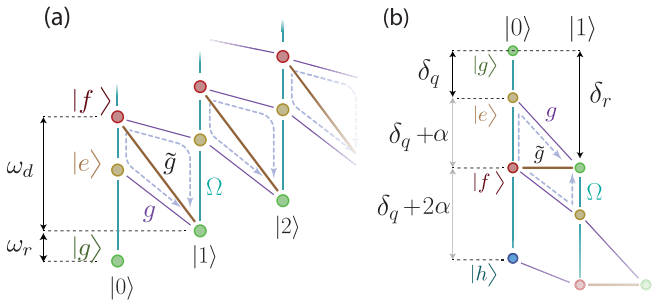

FIG. 2. (Color online) Schematic energy level diagram of the system: (a) in the laboratory frame and (b) in the rotating frame of the drive frequency ω_d, which compensates for the energy difference between $|f0\rangle$ and $|g1\rangle$. The effective tunable coupling $\tilde{g}$ between the bare states $|f0\rangle$ and $|g1\rangle$ can be understood as a second-order cavity-assisted Raman process, indicated by the dashed arrows.

as the sum of an N-level JC term and a coherent drive term, $H = H_{\rm JC} + H_d$. Here [31],

$$H_{\rm JC} = \delta_r a^\dagger a + \delta_q b^\dagger b + \frac{\alpha}{2} b^\dagger b^\dagger b b + g(ab^\dagger + a^\dagger b) \quad (3)$$

and

$$H_d = \frac{\Omega(t)}{2}(e^{i\phi} b + \text{H.c.}), \quad (4)$$

where $\delta_r \equiv \omega_r^0 - \omega_d$ and $\delta_q \equiv \omega_{ge}^0 - \omega_d$ are the resonator-drive and transmon-drive detunings, respectively. ω_r^0 and ω_{ge}^0 denote the bare quantities associated with ω_r and ω_{ge} defined above (Fig. 2). The operator a ($a^\dagger$) is the annihilation (creation) operator for the resonator mode and b ($b^\dagger$) its analog for the transmon $b \equiv |g\rangle\langle e| + \sqrt{2}|e\rangle\langle f| + \sqrt{3}|f\rangle\langle h| + \ldots$ when treated as an anharmonic oscillator at frequency ω_{ge}^0 [31]. A JC-type interaction [39] couples states which have the same total number of excitations, while a coherent drive field with time-dependent amplitude $\Omega(t)$, frequency ω_d, and phase ϕ couples neighboring pairs of transmon states. In the following, we omit the time dependence of $\Omega(t)$ for notational clarity. The above Hamiltonian is valid in the transmon limit where $E_{\rm J}/E_{\rm C} \gg 1$.

We consider the system in the dispersive regime, that is, $\Delta = \omega_{ge} - \omega_r \gg g$. To calculate the tunable effective coupling strength, we rewrite the Hamiltonian H in the eigenbasis of $H_{\rm JC}$ and treat the coherent drive term H_d perturbatively, expanding the solution in powers of the small parameter Ω. Note that $|i,j\rangle_D$ ($i = g,e,f,h,\ldots$ and $j = 0,1,2,\ldots$) is used for the eigenstates of $H_{\rm JC}$, and $|i,j\rangle$ for the bare qubit-resonator states. The drive Hamiltonian H_d can be written in the $|i,j\rangle_D$ basis as

$$H_d = \sum_{ij,kl} \frac{\Omega}{2} |i,j\rangle_D\langle k,l|_D \{\langle i,j|_D (e^{i\phi} b + e^{-i\phi} b^\dagger)|k,l\rangle_D\}.$$

When the resonance condition in Eq. (1) is satisfied the main contribution to the evolution of the system comes from the terms coupling the resonant states $|g,l+1\rangle_D$ and $|f,l\rangle_D$, while the terms describing off-resonant transitions in Eq. (5) can be neglected. With this rotating-wave-type approximation, the drive Hamiltonian becomes

$$H_d \approx \sum_l \frac{\Omega}{2} |g,l+1\rangle_D\langle f,l|_D \times \{\langle g,l+1|_D (e^{i\phi} b + e^{-i\phi} b^\dagger)|f,l\rangle_D\}. \quad (5)$$

To show that the effective coupling between the transmon and the resonator is indeed of the JC type, we note that the dressed states $|f,l\rangle_D$ and $|g,l+1\rangle_D$ are given, up to first order in g, by

$$|f,l\rangle_D = |f,l\rangle - \frac{g\sqrt{2(l+1)}}{\Delta+\alpha}|e,l+1\rangle + \frac{g\sqrt{3l}}{\Delta+2\alpha}|h,l-1\rangle, \quad (6)$$

$$|g,l+1\rangle_D = |g,l+1\rangle + \frac{g\sqrt{l+1}}{\Delta}|e,l\rangle, \quad (7)$$

where the coupling $g(ab^\dagger + a^\dagger b)$ is considered a perturbation to the uncoupled transmon-resonator system [i.e., $(g/\Delta)^2 \ll 1$]. Using this approximation for the dressed states, we calculate the matrix element

$$\tilde{g}_l \equiv \langle g,l+1|_D H_d |f,l\rangle_D \approx g\Omega e^{i\phi} \sqrt{\frac{l+1}{2}} \frac{\alpha}{\Delta(\Delta+\alpha)}, \quad (8)$$

which represents the coupling strength between dressed states $|f,l\rangle_D$ and $|g,l+1\rangle_D$. As expected, $\tilde{g}_l$ is tunable in both phase and amplitude because of its dependence on the complex drive strength $\Omega e^{i\phi}$.

Next, defining the qubit raising and lowering operators

$$\tilde{\sigma} \equiv \sum_l |g,l\rangle_D\langle f,l|_D, \tilde{\sigma}^\dagger \equiv \sum_l |f,l\rangle_D\langle g,l|_D \quad (9)$$

and the dressed photon annihilation operator

$$\tilde{a} \equiv \sum_{l,j} \sqrt{l+1}|j,l\rangle_D\langle j,l+1|_D, \quad (10)$$

the drive Hamiltonian in Eq. (5) can be written in the JC form

$$\tilde{H}_d \approx \tilde{g}\tilde{a}^\dagger\tilde{\sigma}_l + \tilde{g}^*\tilde{a}\tilde{\sigma}_l{}^\dagger, \quad (11)$$

with $\tilde{g} \equiv \tilde{g}_0 \approx g\Omega e^{i}\phi\alpha/(\sqrt{2}\Delta(\Delta+\alpha))$. The absolute value of the coupling $\tilde{g}$ in Eq. (11) describes the splitting observed in Fig. 1(c).

It is instructive to compare the tunable transmon-resonator coupling $\tilde{g}$ to the effective coupling $g_\Lambda = g\Omega e^{i}\phi/\Delta$ between the two degenerate states of a Λ system obtained from the adiabatic elimination technique [25,27,30,41]. Most notably, the coupling strength for the transmon-resonator system is lower than that of the Λ system, $\tilde{g} < g_\Lambda$. This result follows from the opposite signs of perturbative contributions from $|e,l\rangle$ and $|e,l+1\rangle$ in Eqs. (6) and (7). Physically, this effect arises from the destructive interference of the two second-order transition paths that couple degenerate levels $|f0\rangle_D$ and $|g1\rangle_D$ (Fig. 2). Indeed, the only reason that the coupling $\tilde{g}$ does not vanish completely is the anharmonicity α of the transmon qubit, which results in a difference in the magnitude of perturbative contributions from $|e,l\rangle$ and $|e,l+1\rangle$. On the other hand, in a Λ system, there is only one transition path

coupling the degenerate levels, and consequently there are no interference effects. The correspondence between the Λ and the transmon systems is easy to see in the limit of large anharmonicity, when $\tilde{g}(\alpha \to \infty) = g_\Lambda$.

As shown in Fig. 1(c), the first-order perturbation theory gives a satisfactory approximation to the tunable transmon-resonator coupling for low drive amplitudes which satisfy $(\Omega/2(\Delta+\alpha))^2 \ll 1$. However, the approximation to $\tilde{g}$ breaks down when this inequality is no longer satisfied, and the first-order approximations to $|f0\rangle_D$ and $|g1\rangle_D$ in Eqs. (6) and (7) lose their validity. In particular, we observe in the experiment that the first-order approximation starts to break down as $\Omega/2\pi$ is increased above approximately 0.2 GHz for $\Delta/2\pi = 0.979$ GHz, i.e., $(\Omega/2(\Delta+\alpha))^2 \approx 0.025$.

IV. AC STARK SHIFT AND DRIVE POWER CALIBRATION

To determine the conversion factor between the applied drive power and the drive amplitude Ω seen by the transmon qubit we fit the observed Stark shift to a perturbative expression for Δ_{f0g1}, where all the parameters other than Ω can be determined from separate measurements. In the following, we discuss the resolvent method used to obtain such a perturbative expression for Δ_{f0g1}.

The resolvent method allows for a systematic approximation of Δ_{f0g1} for increasing orders of interaction in both g and Ω. The Hamiltonian $H = H_0 + H_I$ consists of a bare part H_0 and an interaction part H_I and its resolvent is defined as [42]

$$G(z) = \frac{1}{z - H}, \tag{12}$$

where z is a complex variable. In particular, the eigenenergies of H are given by the poles of $G(z)$. Specifically, for our transmon-resonator system, we split the driven JC Hamiltonian given by Eqs. (3) and (4) into

$$H_0 = \delta_r a^\dagger a + \delta_q b^\dagger b + \frac{\alpha}{2} b^\dagger b^\dagger b b \tag{13}$$

and

$$H_I = g\, a b^\dagger + \frac{\Omega(t)}{2} e^{i\phi} b + \text{H.c.}, \tag{14}$$

where g and Ω are real numbers. With this notation, we can rewrite the resolvent as

$$G(z) = \frac{1}{z - H_0} \sum_{n=0}^{\infty} \left(\frac{H_I}{z - H_0} \right)^n. \tag{15}$$

If the states $|\phi_i\rangle$ and $|\phi_j\rangle$ are two degenerate eigenvectors of the bare Hamiltonian satisfying $H_0|\phi_{i,j}\rangle = E|\phi_{i,j}\rangle$, the resolvent operator restricted to the two-dimensional space spanned by them can be written in the final form

$$G(z) = \frac{1}{z - H_0 - \Sigma(z)}, \tag{16}$$

where the operators H_0 and $\Sigma(z)$ are to be understood as acting on the two-dimensional space and the matrix elements $\Sigma_{kl}(z) = \langle\phi_k|\Sigma(z)|\phi_l\rangle$ for $k,l \in \{i,j\}$ are given by

$$\begin{aligned}\Sigma_{kl}(z) = {} & \langle\phi_k|H_I|\phi_l\rangle + \sum_{m\neq i,j} \langle\phi_k|H_I|\phi_m\rangle \frac{1}{z - E_m} \langle\phi_m|H_I|\phi_l\rangle \\ & + \sum_{m,m'\neq i,j} \langle\phi_k|H_I|\phi_m\rangle \frac{1}{z - E_m} \langle\phi_m|H_I|\phi_{m'}\rangle \\ & \times \frac{1}{z - E'_m} \langle\phi_{m'}|H_I|\phi_l\rangle + \cdots,\end{aligned} \tag{17}$$

which is the weighted sum of all transition paths coupling states $|\phi_k\rangle$ and $|\phi_l\rangle$ through intermediate bare eigenstates $\{|\phi_m\rangle\}_{m=1}^{\infty}$ excluding $|\phi_i\rangle$ and $|\phi_j\rangle$. Equation (16) is obtained by inserting an appropriate number of copies of the identity $\mathbb{I} = \sum_m |\phi_m\rangle\langle\phi_m|$ into each term of the sum in Eq. (15) and by noting that the identity

$$\begin{aligned}&\langle\phi_k| \left(\frac{1}{z - H_0} \sum_{n=0}^{\infty} \left(\frac{H_I}{z - H_0} \right)^n \right) |\phi_l\rangle \\ &\quad = \langle\phi_k| \left(\frac{1}{z - H_0} \sum_{n=0}^{\infty} \left(\frac{\Sigma}{z - H_0} \right)^n \right) |\phi_l\rangle\end{aligned} \tag{18}$$

holds if $k,l \in \{i,j\}$.

Equation (16) shows that $H_0 + \Sigma(z)$ can be interpreted as an effective Hamiltonian $H^{\text{eff}}(z)$ describing the evolution of the system in the two-dimensional subspace spanned by $|\phi_i\rangle$ and $|\phi_j\rangle$. The resonance condition, (1), which corresponds to the avoided crossing in Fig. 1(c), can now be expressed as

$$z - H^{\text{eff}}_{g1g1}(z) = z - H^{\text{eff}}_{f0f0}(z) = 0,$$

which is to be satisfied when the bare energies E_{f0} and E_{g1} are separated by a detuning $\Delta_{f0g1}(\Omega) + \Delta_{\text{JC}}$. Here the constant term Δ_{JC} represents the Ω-independent renormalization of the bare energies due to the JC coupling g only, such that $\Delta_{f0g1}(0) = 0$. Thus, we can calculate the detuning $\Delta_{f0g1}(\Omega)$ by iteratively solving the coupled equations

$$\begin{aligned}&z - E_{g1} - \Sigma_{g1g1}(z,\Omega) = 0, \\ &z - E_{g1} + \Delta_{f0g1}(\Omega) + \Delta_{\text{JC}} - \Sigma_{f0f0}(z,\Omega) = 0,\end{aligned} \tag{19}$$

with the initial value $z = 0$. Fitting the resulting expression for $\Delta_{f0g1}(\Omega)$ to the experimental data (see Fig. 3) provides the conversion factor k between the applied drive power and the drive amplitude Ω seen by the transmon. This conversion factor is also used to compute the qubit drive strength value in Fig. 1(c), giving a good agreement between our measurement and the perturbation theory calculation.

V. NUMERICAL AND ANALYTICAL RESULTS ON TIME-DEPENDENT VACUUM RABI OSCILLATIONS

An effective transmon-resonator coupling leads to a coherent exchange of excitations (SWAP) between states $|f,l\rangle_D$ and $|g,l+1\rangle_D$. Achieving a high fidelity for this SWAP operation is crucial for further applications of the microwave-induced transmon-resonator coupling in the context of quantum computing. In this section, first we derive an analytical expression for the fidelity of the SWAP operation when the external drive is turned on and off instantaneously. Then we use numerical simulations to account for the effects arising from pulse

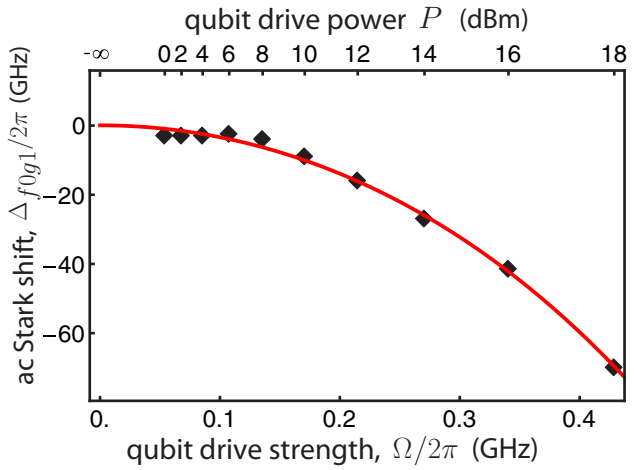

FIG. 3. (Color online) Measured values of Δ_{f0g1} for increasing drive amplitudes Ω. A fit to the expression in Eq. (20) obtained from the resolvent method (solid line) where the perturbative series is truncated at the the sixth order in Ω. The fit gives the conversion factor between the applied drive power and the applied drive amplitude seen by the transmon. The scale at the top indicates the drive power at the signal generator, where each tick stands for the drive power at which the data point is obtained.

profiles that vary slowly with respect to Δ. We conclude that the SWAP operation can be realized with a very high fidelity for realistic pulse profiles.

When the drive is turned on and off instantaneously, one can derive an analytical expression for the Rabi oscillations in the population in $|g1\rangle_D$, given the initial state $|f0\rangle_D$. The population in $|g1\rangle_D$ at time t, denoted $P_{g1D}(t)$, is given by the modulus square of the overlap between the time-evolved initial state $|f0(t)\rangle_D$ and the target state $|g1\rangle_D$,

$$P_{g1D}(t) = |\langle g1|_D\, |f0(t)\rangle_D|^2\,, \tag{20}$$

where $|f0(t)\rangle_D = U(t)|f0\rangle_D$, with the unitary time evolution operator $U(t) \equiv \mathrm{e}^{-\mathrm{i}}Ht$.

To express $P_{g1D}(t)$ in a convenient form, we expand the initial and target states in the eigenbasis of the full Hamiltonian,

$$|f0\rangle_D = \sum_n \alpha_n |\Phi_n\rangle, \tag{21}$$

$$|g1\rangle_D = \sum_n \beta_n |\Phi_n\rangle, \tag{22}$$

where the eigenstates $|\Phi_n\rangle$ satisfy $H|\Phi_n\rangle = \epsilon_n|\Phi_n\rangle$, and the coefficients α_n and β_n are defined as $\langle\Phi_n|f0\rangle_D$ and $\langle\Phi_n|g1\rangle_D$, respectively. In this new basis, the time-dependent population in $|g1\rangle_D$ is

$$P_{g1D}(t) = \sum_n \alpha_n^2\beta_n^2 + 2\sum_{n<m} |\alpha_m^*\beta_m\alpha_n^*\beta_n| \times \cos\left[(\epsilon_n - \epsilon_m)t + \theta_{nm}\right], \tag{23}$$

where θ_{nm} is the phase of $(\alpha_m^*\beta_m\alpha_n^*\beta_n)$.

Equation (23) is an exact and useful relation between the solution to the full Hamiltonian (which can be approximated using perturbation theory) and the rate and fidelity of the population exchange between $|f0\rangle_D$ and $|g1\rangle_D$. In particular, the maximum fidelity $\mathcal{F}$ of the SWAP operation between $|f0\rangle_D$ and $|g1\rangle_D$ can be extracted from Eq. (23) as $\mathcal{F} = 4|\alpha_+\alpha_-\beta_+\beta_-|$, and its rate as $2\tilde{g} = \epsilon_+ - \epsilon_-$, where the subscripts $\pm$ stand for the two eigenstates of H which have the largest overlaps with $|f0\rangle_D$ and $|g1\rangle_D$. We denote these eigenstates $|\Phi_\pm\rangle$. When the resonance condition in Eq. (1) is satisfied and there are no other states whose energies are close to that of $|f0\rangle_D$ or $|g1\rangle_D$, i.e., $(\Omega/2/(\Delta+\alpha))^2 \ll 1$, these eigenstates are simply the two polariton states $|\Phi_\pm\rangle = 1/\sqrt{2}\,(|f0\rangle_D \pm |g1\rangle_D)$. In this weak drive limit, Eq. (23) implies that the population exchange between $|f0\rangle_D$ and $|g1\rangle_D$ occurs with unit fidelity $\mathcal{F} = 1$.

For realistic amplitudes and detunings a reduction in $\mathcal{F}$ is caused by the population leakage out of the initial and target states. To calculate the Ω dependence of the fidelity, we use the second-order corrections to the eigenstates $|\Phi_\pm\rangle$ induced by the perturbation $\tilde{H}_d$ (see Appendix B). As a result, the fidelity of the SWAP operation between $|f0\rangle_D$ and $|g1\rangle_D$ is

$$\mathcal{F} = 1 - \left(\left(\frac{\Omega/2}{\Delta+\alpha}\right)^2 + \left(\frac{\sqrt{2}\Omega/2}{\Delta}\right)^2 + \left(\frac{\sqrt{3}\Omega/2}{\Delta-\alpha}\right)^2\right), \tag{24}$$

up to second order in Ω/Δ. Note that the reduction in fidelity is caused by population leakage out of states $|f0\rangle_D$ and $|g1\rangle_D$ to neighboring states. We observe that the simulated fidelity shown in Fig. 4(a) for a drive pulse with zero rise time is in good agreement with the analytical calculation in Eq. (24). The simulation of the transmon dynamics in the absence of decoherence was performed by solving the Schrödinger equation with the Hamiltonian given by Eqs. (3) and (4). The underlying Hilbert space was truncated to four energy levels of the transmon and four Fock states of the resonator.

The calculation above is based on the assumption that the drive pulse is turned on and off instantaneously and the obtained fidelity is therefore valid in the limit of an ideal square pulse. If, however, the pulse is ramped up and down gradually, the process becomes adiabatic with respect to the off-resonant transitions. Simulation results presented in Fig. 4 show that this effect improves the fidelity significantly.

The shape of the drive pulse $\Omega(t)$ for the simulations is chosen such that the effective coupling $\tilde{g}(t)$ has the form

$$\begin{aligned}
\tilde{g}(t) &= \tilde{g}_{\max} && \text{for } \Delta t < t < T - \Delta t,\\
&= \tilde{g}_{\max}\sin^2(\pi t/2\Delta t) && \text{for } t \leqslant \Delta t,\\
&= \tilde{g}_{\max}\sin^2(\pi(T-t)/2\Delta t) && \text{for } t \geqslant T - \Delta t,
\end{aligned}$$

where T denotes the length of the pulse, Δt is the rise time, and the amplitude $\tilde{g}_{\max}$ is chosen such that $\int_0^T \tilde{g}(t)\,\mathrm{d}t = \pi/2$, resulting in a π flip between states $|f0\rangle_D$ and $|g1\rangle_D$. The frequency of the pulse is varied in time to exactly cancel the variations in the amplitude-dependent ac Stark shift.

To generate the correct drive pulse for the simulation, we needed to calculate the ac Stark shift and the effective coupling $\tilde{g}$ with a good accuracy. For this reason, we decided to use a numerical procedure based on diagonalization of the Hamiltonian, which is described in more detail in Appendix A. While this method is more accurate than the analytical expression obtained using perturbation theory, the latter is a

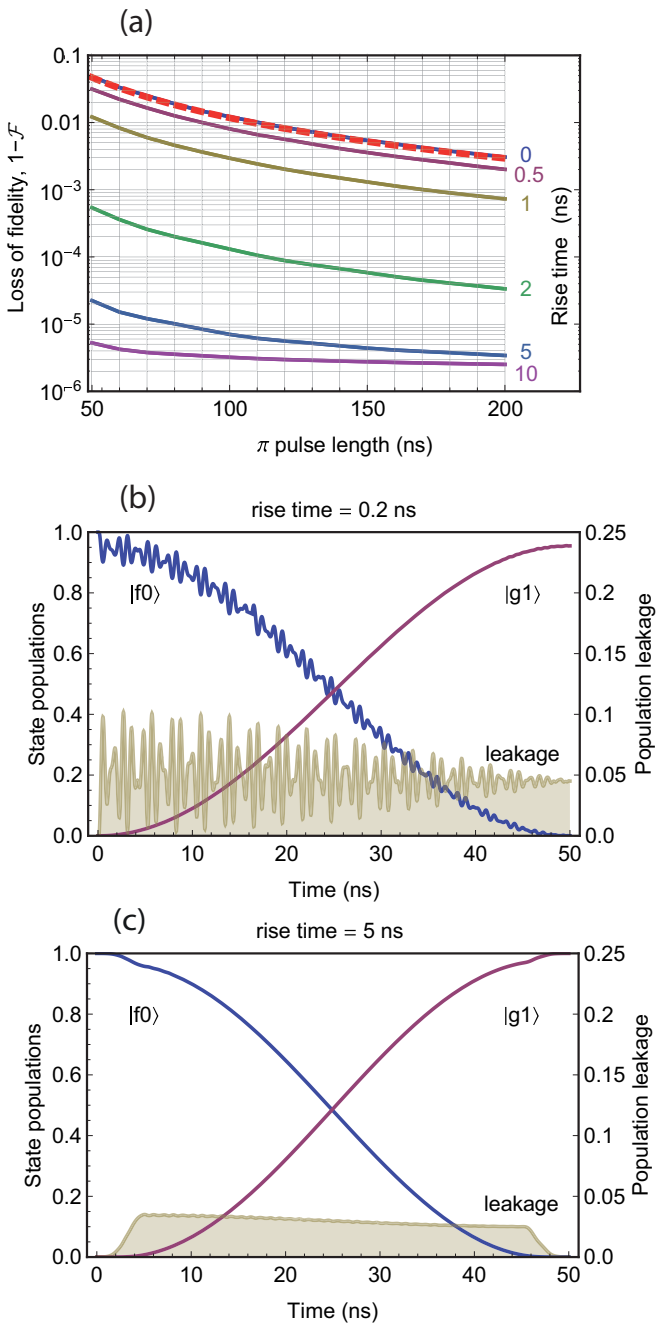

FIG. 4. (Color online) (a) Dependence of the loss of fidelity $1-\mathcal{F}$ on the length of the π pulse and its rise time. The transmon-resonator detuning is set to $\Delta/2\pi = 0.979$ GHz, the anharmonicity is $\alpha/2\pi = -0.376$ GHz, and $g/2\pi = 65$ MHz. Solid lines show the results of the numerical simulations. The theoretical prediction of Eq. (24) is shown by the dashed (red) line. (b, c) Time evolution of the populations p_{f0}, p_{g1} in $|f0\rangle_D, |g1\rangle_D$ and leakage to other levels given by $1-p_{g1}-p_{f0}$ for a 50-ns drive pulse with rise times of 0.2 ns (b) and 5.0 ns (c).

more time-efficient way of determining the behavior of ac Stark shift as a function of other system parameters (i.e., Δ, α, and g).

With pulses generated by this method, the simulations show that the population SWAP between $|f0\rangle_D$ and $|g1\rangle_D$ can be realized with essentially unit fidelity (>0.99999) when decoherence is neglected. In current state-of-the-art experiments, the achievable fidelities will therefore be limited mainly by the coherence times of the transmons or imperfections in the generated drive pulses.

VI. CONCLUSION

In conclusion, we have experimentally demonstrated a cavity-assisted Raman process to realize a tunable transmon-resonator coupling in a superconducting circuit QED architecture. This effective coupling is induced by coherently driving a transmon qubit. Its maximal value is determined by the maximum drive power that can be applied to the qubit without violating one of the underlying assumptions, such as adiabaticity with respect to unwanted off-resonant transitions or the rotating-wave approximation for the drive term. The measured data are in very good agreement with a perturbative calculation of the coupling strength $\tilde{g}$ between $|f0\rangle_D$ and $|g1\rangle_D$. Our calculations show that the strength of the Raman transition is reduced in comparison to the one implemented in a Λ-level system [25,29] by the destructive interference between the two second-order transition paths which couple $|f0\rangle_D$ and $|g1\rangle_D$.

We also determined the fidelity of the SWAP operation which utilized the cavity-assisted Raman process, by both numerical and analytical means. A second-order degenerate perturbation calculation shows that the fidelity of the population exchange strongly depends on the population leakage from $|f0\rangle_D$ and $|g1\rangle_D$ to the closest lying states [see Eq. (24)], a result which is also supported by numerical simulations (Fig. 4). We found that the fidelity of the SWAP operation is expected to be very close to unity in the absence of a decoherence effect and, in realistic systems, will most likely be limited by the coherence time of the transmon.

ACKNOWLEDGMENTS

We would like to thank Alexandre Blais and Simone Gasparinetti for useful comments on the manuscript. This work was supported by Swiss National Science Foundation Project 150046, by the National Center of Competence in Research "Quantum Science and Technology," and by ETH Zurich.

S.Z. and M.P. contributed equally to this work.

APPENDIX A: NUMERICAL CALCULATION OF THE AC STARK SHIFT

In this Appendix, we describe the evolution of the transmon under the approximation of slowly varying drive pulses. We then define the ac Stark shift operationally as the shift of the drive frequency required to implement a perfect SWAP between states $|f0\rangle_D$ and $|g1\rangle_D$. Finally, we describe a method for calculating the ac Stark shift numerically.

If the drive amplitude $\Omega(t)$ is varied slowly compared to the energy separation of $|f0\rangle_D$ and $|g1\rangle_D$ from other energy eigenstates, the system evolves adiabatically with respect to the off-resonant transitions. Therefore, if the system is initially prepared in a superposition of $|f0\rangle_D$ and $|g1\rangle_D$, it remains at all times in the subspace $\mathcal{S}(\Omega)$ spanned by the two instantaneous

eigenstates $|\Phi_1(\Omega)\rangle$ and $|\Phi_2(\Omega)\rangle$ corresponding to $|f0\rangle_D$ and $|g1\rangle_D$.

To describe the evolution of the state vector $|\Psi(t)\rangle$ in $\mathcal{S}(\Omega)$, we first introduce a mapping which connects the subspaces $\mathcal{S}(\Omega)$ for different values of Ω. Using this transformation, the action of the full Hamiltonian for any Ω is mapped to an effective Hamiltonian acting on $\mathcal{S}(0)$, that is, the subspace spanned by $|f0\rangle_D$ and $|g1\rangle_D$. Using this formalism, we calculate the Stark shift as the shift of the drive frequency needed to keep the effective Hamiltonian in the "resonant form" $\tilde{g}\sigma_x \equiv \tilde{g}(|f0\rangle_D\langle g1|_D + \text{H.c.})$. If the drive frequency is not adjusted, the effective Hamiltonian contains a term proportional to σ_z which prevents us from realizing a perfect SWAP operation between the two states.

We start by introducing a linear map, $M_\Omega : \mathcal{S}(0) \to \mathcal{S}(\Omega)$, defined as

$$M_\Omega = \lim_{\Delta\Omega\to 0} P(\Omega)P(\Omega-\Delta\Omega)\dots P(2\Delta\Omega)P(\Delta\Omega)P(0), \tag{A1}$$

where $P(\Omega) = \sum_{i=1,2} |\Phi_i(\Omega)\rangle\langle\Phi_i(\Omega)|$ is a projector onto $\mathcal{S}(\Omega)$. This map represents a continuous series of projections onto the subspaces $\mathcal{S}(x)$ for x varying from 0 to Ω.

As the state vector $|\Psi(t)\rangle$ evolves adiabatically and therefore lies in $\mathcal{S}(\Omega(t))$, we can write it in the form

$$|\Psi(t)\rangle = M_{\Omega(t)}|\psi(t)\rangle,$$

where $|\psi(t)\rangle$ is some vector evolving in the subspace $\mathcal{S}(0)$ spanned by $|f0\rangle_D$ and $|g1\rangle_D$. In this way, we have reduced the problem of finding the evolution of the state vector $|\Psi(t)\rangle$ in a changing subspace $\mathcal{S}(\Omega(t))$ to that of finding the evolution of the directly related vector $|\psi(t)\rangle$ in a fixed subspace $\mathcal{S}(0)$.

Since $|\Psi(t+\mathrm{d}t)\rangle$ lies in $\mathcal{S}(\Omega(t+\mathrm{d}t))$, it can be expressed as

$$\begin{aligned}|\Psi(t+\mathrm{d}t)\rangle =& P(\Omega(t+\mathrm{d}t))|\Psi(t+\mathrm{d}t)\rangle\\ =& P(\Omega(t+\mathrm{d}t))\exp(-\mathrm{i}H(t)\mathrm{d}t)|\Psi(t)\rangle,\end{aligned}$$

resulting in the following evolution equation for $|\psi(t)\rangle$:

$$\begin{aligned}&M_{\Omega(t+\mathrm{d}t)}|\psi(t+\mathrm{d}t)\rangle\\ &\quad= P(\Omega(t+\mathrm{d}t))\exp(-\mathrm{i}H(t)\mathrm{d}t)M_{\Omega(t)}|\psi(t)\rangle.\end{aligned} \tag{A2}$$

Under the reasonable assumption that the subspace $\mathcal{S}(\Omega)$ changes smoothly with Ω, it can be shown that M_Ω preserves vector norms in $\mathcal{S}(\Omega)$. It follows that $M_\Omega^\dagger$, which is an infinite product of projectors analogous to M_Ω but in the reverse order, is the inverse of M_Ω. Hence, after dropping the projector $P(\Omega(t+\mathrm{d}t))$ from the right-hand side of Eq. (A2) as well as from the product form of $M_{\Omega(t+\mathrm{d}t)}$ [cf. Eq. (A1)] on its left-hand side, we multiply the equation by $M_{\Omega(t)}^\dagger$ to obtain

$$|\psi(t+\mathrm{d}t)\rangle = M_{\Omega(t)}^\dagger \exp(-\mathrm{i}H(t)\mathrm{d}t)M_{\Omega(t)}|\psi(t)\rangle,$$

which we transform into the differential form

$$\frac{\mathrm{d}}{\mathrm{d}t}|\psi(t)\rangle = -\mathrm{i}M_{\Omega(t)}^\dagger H(t) M_{\Omega(t)}|\psi(t)\rangle.$$

The evolution of the vector $|\psi(t)\rangle$ is therefore governed by the effective Hamiltonian

$$H_{\text{eff}}(t) = M_{\Omega(t)}^\dagger H(t) M_{\Omega(t)} \tag{A3}$$

acting on $\mathcal{S}(0)$, resulting in the evolution operator $U(t_\mathrm{f},t_\mathrm{i}) = \mathcal{T}\exp\int_{t_\mathrm{i}}^{t_\mathrm{f}}(-\mathrm{i}H_{\text{eff}}(t))\,\mathrm{d}t$. If we assume that the drive amplitude at the initial time t_i and the final time t_f is 0, we have $M_{\Omega(t_\mathrm{i})} = M_{\Omega(t_\mathrm{f})} = P(0)$ and hence $|\psi(t_\mathrm{i})\rangle = |\Psi(t_\mathrm{i})\rangle$ and $|\psi(t_\mathrm{f})\rangle = |\Psi(t_\mathrm{f})\rangle$. Then we can directly write down the evolution from $|\Psi(t_\mathrm{i})\rangle$ to $|\Psi(t_\mathrm{f})\rangle$:

$$|\Psi(t_\mathrm{f})\rangle = U(t_\mathrm{f},t_\mathrm{i})|\Psi(t_\mathrm{i})\rangle.$$

This result allows us to determine the ac Stark shift as the amplitude-dependent shift of the drive frequency needed to realize a perfect SWAP operation between $|f0\rangle_D$ and $|g1\rangle_D$. For this, the effective Hamiltonian has to have the form

$$H_{\text{eff}}(t) = E_{\text{offset}}(t)\mathbb{1} + \tilde{g}(t)(|f0\rangle_D\langle g1|_D + \text{H.c.}), \tag{A4}$$

where the overall energy shift $E_{\text{offset}}(t)$ leading only to an overall phase shift is omitted since it is physically irrelevant. This equation is equivalent to the requirement that the equal superposition states $|\varphi_{1,2}\rangle = (|f0\rangle_D \pm |g1\rangle_D)/\sqrt{2}$ are eigenstates of $H_{\text{eff}}(t)$ and therefore, by virtue of Eq. (A3), that $M_{\Omega(t)}|\varphi_{1,2}\rangle$ are eigenstates of $H(t)$ which we have previously denoted $|\Phi_{1,2}(\Omega)\rangle$. In other words,

$$|\Phi_i(\Omega)\rangle = M_\Omega|\varphi_i\rangle. \tag{A5}$$

This equation can be solved for M_Ω. However, since our goal is to determine the ac Stark shift, we need an equation for the Hamiltonian instead. To get it, we transform Eq. (A5) into a differential form. By substituting $\Omega \to \Omega + \mathrm{d}\Omega$, we find the relation between $|\Phi_i(\Omega+\mathrm{d}\Omega)\rangle$ and $|\Phi_i(\Omega)\rangle$,

$$|\Phi_i(\Omega+\mathrm{d}\Omega)\rangle = P(\Omega+\mathrm{d}\Omega)|\Phi_i(\Omega)\rangle,$$

which, after multiplication by $\langle\Phi_j(\Omega+\mathrm{d}\Omega)|$, we write in the form

$$\langle\Phi_i(\Omega)|\frac{\mathrm{d}}{\mathrm{d}\Omega}|\Phi_j(\Omega)\rangle = 0.$$

The associated initial condition follows from substituting $\Omega = 0$ into Eq. (A5), giving $|\Phi_{1,2}(0)\rangle = (|f0\rangle_D \pm |g1\rangle_D)/\sqrt{2}$. Therefore, the two equal superposition states have to be eigenstates of the nondriven Hamiltonian. This is, by definition, also true for $|f0\rangle_D$ and $|g1\rangle_D$. The only way the two distinct pairs of vectors can be eigenstates at the same time is if the subspace they are spanning is degenerate. This can be achieved by choosing the correct frequency of the rotating frame, giving us a condition for the drive frequency at $\Omega = 0$.

For $i = j$, the differential equation above can be satisfied simply by choosing the correct phase of the eigenstates $|\Phi_{1,2}(\Omega)\rangle$. After expressing the derivative of the eigenstate in terms of the derivative of the Hamiltonian, the remaining equations for $i \neq j$ are equivalent to

$$\langle\Phi_1(\Omega)|\frac{\mathrm{d}H(\Omega)}{\mathrm{d}\Omega}|\Phi_2(\Omega)\rangle = 0.$$

Now we consider that the Hamiltonian depends on Ω not only directly but also through the amplitude-dependent drive frequency $\omega_d(\Omega)$. The total derivative with respect to Ω can then be expressed using the chain rule, leading to

the equation

$$\langle\Phi_1(\Omega,\omega_d)|\frac{\partial H(\Omega,\omega_d)}{\partial\Omega}|\Phi_2(\Omega,\omega_d)\rangle + \frac{\mathrm{d}\omega_d(\Omega)}{\mathrm{d}\Omega}\langle\Phi_1(\Omega,\omega_d)|\frac{\partial H(\Omega,\omega_d)}{\partial\omega_d}|\Phi_2(\Omega,\omega_d)\rangle = 0. \tag{A6}$$

We can solve this differential equation for $\omega_d(\Omega)$ numerically to find the amplitude-dependent drive frequency which yields an effective Hamiltonian of the form shown in Eq. (A4).

The simple procedure for finding the solution is summarized here:

(1) Start with $\Omega = 0$. Find ω_d by requiring $|f0\rangle_D$ and $|g1\rangle_D$ to be degenerate.

(2) Find the eigenstates $|\Phi_{1,2}(\Omega,\omega_d)\rangle$ of the Hamiltonian $H(\Omega,\omega_d)$. For the first step, when $\Omega = 0$ and the eigenstates are degenerate, choose $|\Phi_{1,2}(\Omega,\omega_d)\rangle = (|f0\rangle_D \pm |g1\rangle_D)/\sqrt{2}$.

(3) Use Eq. (A6) to calculate $\omega_d'(\Omega) := \mathrm{d}\omega_d(\Omega)/\mathrm{d}\Omega$

(4) Set $\omega_d \to \omega_d + \omega_d'(\Omega)\Delta\Omega$ and $\Omega \to \Omega + \Delta\Omega$.

(5) Go to step 2.

Once the solution is known, the effective coupling $\tilde{g}(\Omega)$ is calculated from the eigenenergies $E_{1,2}(\Omega,\omega_d)$ of the two eigenstates $|\Phi_{1,2}(\Omega,\omega_d)\rangle$. Inspection of Eq. (A4) shows that these eigenenergies are equal to $E_{\mathrm{offset}} \pm \tilde{g}$ and therefore

$$\tilde{g}(\Omega) = \frac{E_1(\Omega,\omega_d) - E_2(\Omega,\omega_d)}{2}.$$

APPENDIX B: CALCULATION OF $\alpha_\pm$ AND $\beta\pm$

In this Appendix we use perturbation theory to calculate the overlaps $\alpha_\pm$, $\beta_\pm$ of the driven Hamiltonian eigenstates $|\Phi_\pm\rangle$ corresponding to the undriven eigenstates $|\Phi_\pm^{(0)}\rangle = (|f0\rangle_D + |g1\rangle_D)/\sqrt{2}$. The result is then used to derive Eq. (24). We retain only terms up to second order in the drive strength Ω and zeroth order in the JC coupling g. In this approximation, we can treat states with different numbers of photons as decoupled and replace the dressed states $|ij\rangle_D$ with the corresponding bare states $|ij\rangle$. The overlaps $\alpha_\pm = \langle\Phi_\pm|f0\rangle$ and $\beta_\pm = \langle\Phi_\pm|g1\rangle$ which we wish to calculate are given by

$$\begin{aligned}\alpha_\pm &= \frac{1}{\sqrt{2}}(1 + \langle\tilde{f0}^{(2)}|f0\rangle) \\ &= \frac{1}{\sqrt{2}}\left(1 - \frac{1}{2}|\langle\tilde{f0}^{(1)}|\tilde{f0}^{(1)}\rangle|^2\right), \\ \beta_\pm &= \pm\frac{1}{\sqrt{2}}(1 + \langle\tilde{g1}^{(2)}|g1\rangle) \\ &= \pm\frac{1}{\sqrt{2}}\left(1 - \frac{1}{2}\langle\tilde{g1}^{(1)}|\tilde{g1}^{(1)}\rangle\right),\end{aligned}$$

where $|\tilde{ij}^{(k)}\rangle$ are the kth-order corrections to the undriven eigenstates $|ij\rangle$. Specifically,

$$\begin{aligned}|\tilde{f0}^{(1)}\rangle &= \frac{\sqrt{3}\Omega/2}{\Delta+\alpha}|h0\rangle - \frac{\sqrt{2}\Omega/2}{\Delta}|e0\rangle, \\ |\tilde{g1}^{(1)}\rangle &= \frac{\Omega/2}{\Delta+\alpha}|e1\rangle,\end{aligned}$$

which results in the following expressions for $\alpha_\pm$ and $\beta_\pm$:

$$\begin{aligned}\alpha_\pm &= \frac{1}{\sqrt{2}}\left(1 - \frac{1}{2}\left(\frac{\sqrt{2}\Omega/2}{\Delta}\right)^2 - \frac{1}{2}\left(\frac{\sqrt{3}\Omega/2}{\Delta-\alpha}\right)^2\right) \\ \beta_\pm &= \pm\frac{1}{\sqrt{2}}\left(1 - \frac{1}{2}\left(\frac{\Omega/2}{\Delta+\alpha}\right)^2\right).\end{aligned} \tag{B1}$$

[1] R. J. Thompson, G. Rempe, and H.-J. Kimble, Phys. Rev. Lett. **68**, 1132 (1992).

[2] R. Miller, T. E. Northup, K. M. Birnbaum, A. Boca, A. D. Boozer, and H.-J. Kimble, J. Phys. B: At. Mol. Opt. Phys. **38**, S551 (2005).

[3] S. Haroche and J.-M. Raimond, *Exploring the Quantum: Atoms, Cavities, and Photons* (Oxford University Press, New York, 2006).

[4] J. P. Reithmaier, G. Sek, A. Loffler, C. Hofmann, S. Kuhn, S. Reitzenstein, L. V. Keldysh, V. D. Kulakovskii, T. L. Reinecke, and A. Forchel, Nature **432**, 197 (2004).

[5] G. Khitrova, H. M. Gibbs, M. Kira, S. W. Koch, and A. Scherer, Nat. Phys. **2**, 81 (2006).

[6] A. Wallraff, D. I. Schuster, A. Blais, L. Frunzio, R.-S. Huang, J. Majer, S. Kumar, S. M. Girvin, and R. J. Schoelkopf, Nature **431**, 162 (2004).

[7] I. Chiorescu, P. Bertet, K. Semba, Y. Nakamura, C. J. P. M. Harmans, and J. E. Mooij, Nature **431**, 159 (2004).

[8] R. J. Schoelkopf and S. M. Girvin, Nature **451**, 664 (2008).

[9] T. Hime, P. A. Reichardt, B. L. T. Plourde, T. L. Robertson, C. E. Wu, A. V. Ustinov, and J. Clarke, Science **314**, 1427 (2006).

[10] R. C. Bialczak, M. Ansmann, M. Hofheinz, M. Lenander, E. Lucero, M. Neeley, A. D. O'Connell, D. Sank, H. Wang, M. Weides *et al.*, Phys. Rev. Lett. **106**, 060501 (2011).

[11] J. M. Gambetta, A. A. Houck, and A. Blais, Phys. Rev. Lett. **106**, 030502 (2011).

[12] S. J. Srinivasan, A. J. Hoffman, J. M. Gambetta, and A. A. Houck, Phys. Rev. Lett. **106**, 083601 (2011).

[13] M. Pechal, L. Huthmacher, C. Eichler, S. Zeytinoglu, A. A. Abdumalikov, S. Berger, A. Wallraff, and S. Filipp, Phys. Rev. X **4**, 041010 (2014).

[14] S. J. Srinivasan, N. M. Sundaresan, D. Sadri, Y. Liu, J. M. Gambetta, T. Yu, S. M. Girvin, and A. A. Houck, Phys. Rev. A **89**, 033857 (2014).

[15] Y. Yin, Y. Chen, D. Sank, P. J. J. O'Malley, T. C. White, R. Barends, J. Kelly, E. Lucero, M. Mariantoni, A. Megrant, C. Neill, A. Vainsencher, J. Wenner, A. N. Korotkov, A. N. Cleland, and J. M. Martinis, Phys. Rev. Lett. **110**, 107001 (2013).

[16] G. Romero, D. Ballester, Y. M. Wang, V. Scarani, and E. Solano, Phys. Rev. Lett. **108**, 120501 (2012).

[17] J. I. Cirac, P. Zoller, H. J. Kimble, and H. Mabuchi, Phys. Rev. Lett. **78**, 3221 (1997).

[18] A. Kuhn, M. Hennrich, and G. Rempe, Phys. Rev. Lett. **89**, 067901 (2002).
[19] D. K. L. Oi, V. Potoček, and J. Jeffers, Phys. Rev. Lett. **110**, 210504 (2013).
[20] I. Fuentes-Guridi, A. Carollo, S. Bose, and V. Vedral, Phys. Rev. Lett. **89**, 220404 (2002).
[21] J. Larson, Phys. Rev. A **83**, 052103 (2011).
[22] S. Bose, A. Carollo, I. Fuentes-Guridi, M. F. Santos, and V. Vedral, J. Mod. Opt. **50**, 1175 (2003).
[23] J. Larson, Phys. Rev. Lett. **108**, 033601 (2012).
[24] J. F. Poyatos, J. I. Cirac, and P. Zoller, Phys. Rev. Lett. **77**, 4728 (1996).
[25] C. C. Gerry and J. H. Eberly, Phys. Rev. A **42**, 6805 (1990).
[26] D. A. Cardimona, V. Kovanis, M. P. Sharma, and A. Gavrielides, Phys. Rev. A **43**, 3710 (1991).
[27] M. Alexanian and S. K. Bose, Phys. Rev. A **52**, 2218 (1995).
[28] Y. Wu, Phys. Rev. A **54**, 1586 (1996).
[29] C. K. Law and H. J. Kimble, J. Mod. Opt. **44**, 2067 (1997).
[30] Y. Wu and X. Yang, Phys. Rev. A **56**, 2443 (1997).
[31] J. Koch, T. M. Yu, J. Gambetta, A. A. Houck, D. I. Schuster, J. Majer, A. Blais, M. H. Devoret, S. M. Girvin, and R. J. Schoelkopf, Phys. Rev. A **76**, 042319 (2007).
[32] R. Bianchetti, S. Filipp, M. Baur, J. M. Fink, C. Lang, L. Steffen, M. Boissonneault, A. Blais, and A. Wallraff, Phys. Rev. Lett. **105**, 223601 (2010).
[33] Y. Shalibo, R. Resh, O. Fogel, D. Shwa, R. Bialczak, J. M. Martinis, and N. Katz, Phys. Rev. Lett. **110**, 100404 (2013).
[34] F. W. Strauch, P. R. Johnson, A. J. Dragt, C. J. Lobb, J. R. Anderson, and F. C. Wellstood, Phys. Rev. Lett. **91**, 167005 (2003).
[35] L. DiCarlo, J. M. Chow, J. M. Gambetta, L. S. Bishop, B. R. Johnson, D. I. Schuster, J. Majer, A. Blais, L. Frunzio, S. M. Girvin *et al.*, Nature **460**, 240 (2009).
[36] A. Fedorov, L. Steffen, M. Baur, M. P. da Silva, and A. Wallraff, Nature **481**, 170 (2012).
[37] A. A. Abdumalikov, J. M. Fink, K. Juliusson, M. Pechal, S. Berger, A. Wallraff, and S. Filipp, Nature **496**, 482 (2013).
[38] H. J. Carmichael, R. J. Brecha, M. G. Raizen, H. J. Kimble, and P. R. Rice, Phys. Rev. A **40**, 5516 (1989).
[39] A. Blais, R.-S. Huang, A. Wallraff, S. M. Girvin, and R. J. Schoelkopf, Phys. Rev. A **69**, 062320 (2004).
[40] L. D. Landau and E. M. Lifshitz, *Quantum Mechanics: Non-relativistic Theory*, Vol. 3 (Pergamon Press, London, 1977).
[41] E. Brion, K. Mølmer, and M. Saffman, Phys. Rev. Lett. **99**, 260501 (2007).
[42] M. Kaku, *Quantum Field Theory: A Modern Introduction* (Oxford University Press, New York, 1993).
[43] V. E. Manucharyan, J. Koch, L. I. Glazman, and M. H. Devoret, Science **326**, 113 (2009).